Research Square

Preprints are preliminary reports that have not undergone peer review.
They should not be considered conclusive, used to inform clinical practice,
or referenced by the media as validated information.

A Phase-Field Simulation Study on Hydraulic Fracturing Roof Cutting for Pressure Relief and Collaborative Control in Gob-Side Entry Retaining of Thick Coal Seams with Hard Roof

Zhijun Xu
China University of Mining and Technology
Chong Li
lichongky@163.com

China University of Mining and Technology
Shuaishuai Jiang
China University of Mining and Technology
Xinlong Ma
China University of Mining and Technology
Yadong Zheng
China University of Mining and Technology
Yue Cao
China University of Mining and Technology

Article

Keywords:

Posted Date: November 17th, 2026

DOI: https://doi.org/10.21203/rs.3.rs-11588234/v1

License: This work is licensed under a Creative Commons Attribution 4.0 International License.
Read Full License

Additional Declarations: No competing interests reported.

A Phase-Field Simulation Study on Hydraulic Fracturing Roof Cutting for Pressure Relief and Collaborative Control in Gob-Side Entry Retaining of Thick Coal Seams with Hard Roof

Zhijun Xu[1], Chong Li*[1], Shuaishuai Jiang[1], Xinlong Ma[1], Yadong Zheng[1], Yue Cao[1]

1. School of Mines, China University of Mining and Technology, Xuzhou, China.

* Correspondence:
Corresponding Author
lichongky@163.com

Abstract: To address long cantilever hanging, stress concentration, and insufficient backfill capacity in gob-side entry retaining (GER) in thick coal seams with a hard roof, a collaborative "pressure relief–support–backfilling" strategy based on directional hydraulic fracturing roof cutting is proposed. COMSOL phase-field simulations are conducted to investigate hydraulic fracture propagation under varying in-situ stress ratios, natural-fracture intersection angles, and cutting parameters. Results show that hydraulic roof cutting reduces the required backfill width by 30%. The optimal parameters are fracture spacing ≥4.5 m, cutting angle 20°, and boreholes oriented along the maximum principal stress. Field application at the N2302 working face of Gucheng Coal Mine shows that floor heave decreases from 670 to 290 mm, roof subsidence from 580 to 230 mm, and rib convergence from 340 to 180 mm, maintaining entry stability.

Keywords: Gob-side entry retaining; Thick coal seam; Hard roof; Hydraulic fracturing; Collaborative control

1 Introduction

Goaf-side roadway retention mining is a pillarless extraction method widely employed in thin- to medium-thick coal seams, significantly increasing coal recovery, reducing abutment pressure at the working face, and mitigating gas accumulation through Y-type ventilation [1-3]. However, when extended to thick coal seams with hard, thick overburden, maintaining tunnel stability becomes markedly challenging [4,5]. Under such conditions, the hard roof behind the goaf tends to form long cantilever beams of 25–40 m; the rotation and subsidence of these cantilevers generate substantial mining-induced stresses, leading to severe roof subsidence, rib spalling, floor heave, and damage to the roadway-adjacent backfill [6-8]. Field observations from typical hard-roof faces in thick coal seams have also been reported in deep mines, confirming that conventional support and filling systems cannot withstand the dynamic loads transmitted by cantilevers [9-11]. Therefore, fundamental modification of the hard-roof structure is required to render goaf-side roadway retention feasible.

Roof-cutting along a predetermined line, i.e., artificially disrupting the continuity of the hard roof, has been widely recognized as an effective measure to mitigate cantilever effects. By establishing a controlled fracture plane, the length of the suspended roof is markedly shortened, and the bending moment borne by the roadway is substantially reduced [12,13]. Early experiments predominantly relied on deep-hole blasting for roof cutting; however, blasting limits directional control, induces substantial disturbances to the existing support system, and poses high safety risks in

high-gas mines. In recent years, hydraulic fracturing has emerged as a more precise and safer alternative technology [14,15]. Hydraulic fracturing generates tensile fractures by injecting high-pressure fluid into the borehole. Compared with blasting, hydraulic fracturing offers superior fracture-direction control, less surrounding-rock damage, and enables continuous operation without interrupting mining activities [16-18].

Several researchers have applied hydraulic fracturing to roof cutting and decompression in hard roofs for goaf-side roadway retention. For example, Wang et al [19] conducted field tests in a medium-thick coal seam and identified that the optimal polyenergy blasting configuration is achieved with a roof-cutting height of 8 m, a cutting angle of 15°, a coal pillar width of 3 m, and a borehole spacing of 800 mm. Huang et al [20] obtained more aggressive cutting parameters under thick coal seam conditions (height 15 m, angle 15°, spacing 500 mm) and observed that the roof collapse after cutting shares the load with the filling wall. Xu et al [21] developed a theoretical model of polyenergy blasting, revealing the relationships among borehole spacing, damage degree, energy absorption coefficient, and blast center distance. Qin et al [22] proposed a deep-hole pre-split blasting scheme with a "4+3+3+3+1" charge configuration (total charge 2800 g), which effectively reduces surrounding rock deformation. In addition, progress has been made in hydraulic roof-cutting technology: Zhang et al [23] constructed a mechanical model to elucidate the pressure-release mechanism and confirmed that directional hydraulic roof cutting significantly reduces roadside support resistance. Wang et al [24] developed a hydraulic softening roof-cutting technique for weakly cemented and water-softening roof conditions in western mining areas, employing high- and low-level double-row water-injection softening boreholes, successfully controlling roof weighting step distance and peak pressure.

Notwithstanding progress, several critical research gaps persist. (1) Systematic quantification of the evolution laws of hydraulically induced fractures under varying geostress environments—particularly the influence of horizontal stress anisotropy on fracture propagation direction—in thick coal seams with hard roofs remains lacking [25,26]. Existing work predominantly relies on empirical or site-specific parameters and has not integrated the geostress field as a design driver within a unified framework. (2) The optimal combination of key cutting-top parameters (spacing between fracture initiation points, top-cut angle, borehole orientation) remains contentious; reported optima vary markedly, and there is no consensus on adjusting these parameters in response to the geostress tensor [27,28]. To address these gaps, this study adopts the N2302 working face of Gucheng Mine as the engineering context, focusing on hydraulic top-cut unloading along the goaf-retained roadway in a thick coal seam with a hard roof. The main surrounding rock failure modes of gob-side entry retaining are summarized, and an “unloading–supporting–filling” synergistic control technology is proposed. COMSOL Multiphysics is employed to analyze the evolution mechanism of hydraulic fractures with the in-situ stress anisotropy ratio and to determine the optimal combination of roof cutting parameters that maximizes fracture connectivity and pressure relief effect; subsequently, field industrial tests are carried out.

2. Engineering background

2.1 Engineering geological condition

The N2302 working face advances in top-coal caving mining along the roof of Seam No. 3, with an average dip of 5° and a burial depth of 530–600 m. It is situated in the Western Wing mining area; to the east lies Working Face N2301, to the north the Western Wing No. 2 return-air roadway, and to the west the N2303 preparatory mining face. As shown in Figure 1, the face length is 302 m; three along-face drifts are arranged for mining and transport: N2302 intake drift, N2302 belt drift, and N2302 return drift, all aligned with the roof of Seam No. 3. The cutting-entry length is 302 m, and the mining span (retreat width) is 688 m. In-situ stress measurements indicate a maximum horizontal principal stress of 18.26 MPa, oriented N55.2°W, a minimum horizontal principal stress of 9.29 MPa, and a vertical principal stress of 13.50 MPa.

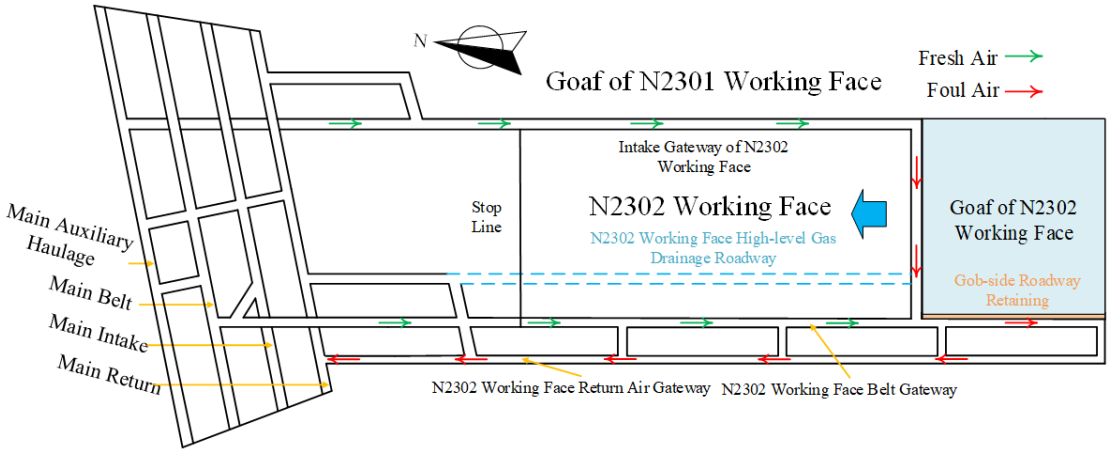


Figure 1. Working-face layout diagram

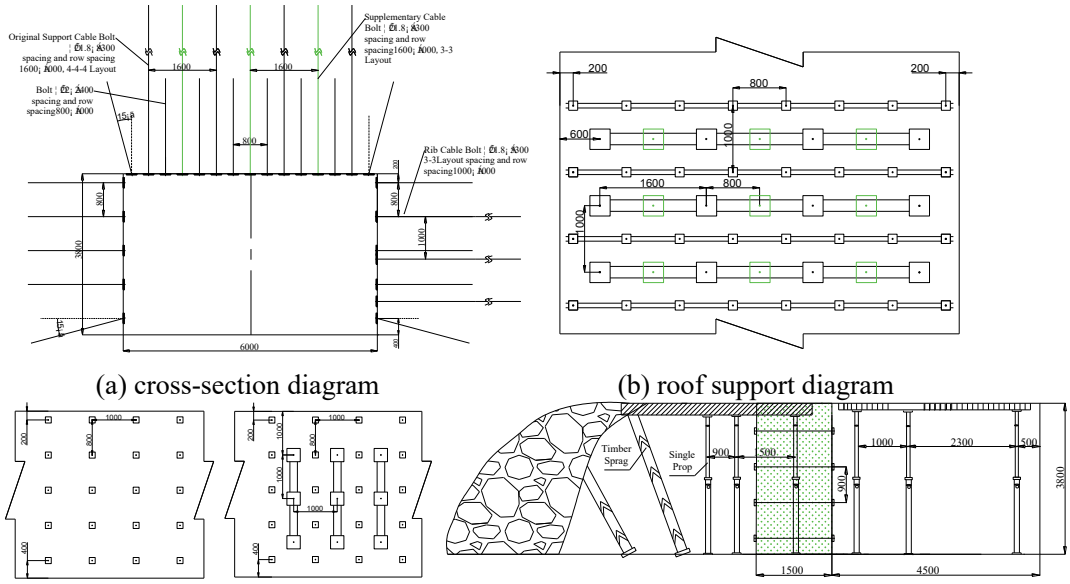
The N2302 working face in the No. 3 coal seam, as depicted in Figure 2, exhibits an average seam thickness of 6.35 m. The immediate roof comprises sandstone, mudstone, and siltstone, with occasional siltstone, averaging 4.03 m in thickness; the main roof consists of medium- to fine-grained sandstone, averaging 5.86 m in thickness. The uniaxial compressive strength is 97.35 MPa, the rock hardness coefficient is 9.7, and the higher-strength lithology is categorized as hard rock. The immediate floor consists of sandy mudstone and mudstone, with occasional siltstone, averaging 0.70 m in thickness. The old floor comprises fine- to medium-grained sandstone, with an average thickness of 3.36 m.

Columnar Section	Lithology	Thickness	Lithology Description
	Fine-grained Sandstone	4.20m	Gray, predominantly quartz with subordinate feldspar, well-sorted, and subrounded.
	Sandy Mudstone	1.95m	Dark gray, thin-bedded, containing plant fossils, with slickensides, and even fracture.
	Mudstone	0.35m	Dark gray, massive, containing plant fossils, with slickensides.
	Sandy Mudstone	1.85m	Dark gray, massive, with sparse plant fossils, semi-hard, uneven fracture.
	Siltstone	1.45m	Dark gray, containing sparse muscovite flakes, with oblique fractures.
	Fine-grained Sandstone	1.55m	Gray, medium-thick bedded, argillaceous cemented, wavy bedding.
	Sandy Mudstone	1.20m	Dark gray, medium-thick bedded, containing sparse plant fossils, semi-hard.
	Medium-grained Sandstone	5.86m	Gray, containing mica flakes, argillaceous cemented, wavy bedding.
	Sandy Mudstone	4.03m	Dark gray, massive, containing plant fossils, uneven fracture.
	Coal Seam No. 3	6.35m	Black, blocky to powdery, predominantly bright coal, semi-bright coal, dull luster.
	Sandy Mudstone	0.7m	Dark gray, medium-thick bedded, containing plant fossils and pyrite, even fracture.
	Fine-grained Sandstone	3.36m	Gray, bedded, wavy bedding, containing siderite concretions, relatively hard.

Figure 2. Bar chart of the roof and floor strata of Coal Seam No. 3

The N2302 working-face belt-entry goaf-side roadway exhibits a rectangular cross-section with an excavation cross-section of 22.80 m^2 (6000 × 3800 mm) and employs anchor-net-beam plus cable support, as shown in Figure 3. The anchor bolt system comprises Φ22 × 2400 mm bolts; top anchors spaced 800 × 1000 mm, eight per

row; auxiliary anchors spaced 800 × 1000 mm, five per row. Cable anchors are Φ21.8 × 8300 mm; top-anchor cables spaced at 1600 × 1000 mm, arranged in a “4-4-4” configuration; strengthening anchor cables spaced at 1600 × 1000 mm, arranged in a “3-3” configuration. Auxiliary anchor cables spacing 1000 × 1000 mm, arranged in a “3-3-3” configuration. The goaf-side roadway employs high-strength soft-form concrete for seamless continuous pouring; soft-form bags are 5000 × 1500 × 3800 mm. Temporary support consists of a one-beam, three-column, large-panel canopy. To enhance wall stability, anchor rods pass through holes in the soft-form bags; the two ends are fitted with steel bands, trays, and screw anchors; anchor spacing is 900 × 900 mm; anchor rods Φ22 × 1850 mm.



(a) cross-section diagram (b) roof support diagram

(c) goaf side (d) coal-side (intact coal) (e) the support of the goaf-side roadway

Figure 3. Belt haulage drift support diagram

2.2 Deformation and Failure Characteristics of Goaf-Adjacent Tunnels

Based on in situ measurements and survey analysis, during the test period, the deformation of the roadway surrounding rock exhibited multiple issues; see Figure 4. The principal observations are as follows: (1) The roof remained in a prolonged hanging condition with no caving, hindering fracture development; (2) The roof bulged, with severe deformation and damage to the supporting components, and several anchor bolts and crown beams lost their load-bearing function, as shown in Figure 4(a)–(d); (3) Locally the backfill tilted, settled, and expanded, effectively losing its bearing capacity; (4) On the coal-seam side, the coal rib bulged outward, the rib-support components failed, and the bottom of the coal rib extruded into the roadway, as shown in Figure 4(e); (5) The roadway displayed asymmetric deformation, with localized roof shear failure and floor heave, and the roadway exhibited pronounced convergence, as shown in Figure 4(f).



(a) (b) (c)



(d) (e) (f)

Figure 4. Deformation and failure of the hard roof of a thick coal seam along the goaf-retained roadway

Field measurements indicate pronounced deformation of the goaf-side retreat roadway roof, floor, and ribs, together with the surrounding rock, as shown in Figure 5. Based on the deformation rate of the retreat roadway surrounding rock behind the working face, the deformation region is divided into three categories: within approximately 50 m behind the face lies a slow-deformation zone with small displacement, slow velocity, and short duration; within approximately 50–200 m behind the face lies a rapid-deformation zone with large displacement, fast velocity, and broad extent; beyond 200 m lies a deformation-stabilized zone with small displacement, slow velocity, and longer extent. The deformation magnitudes are approximately: floor about 670 mm, roof about 580 mm, and ribs about 340 mm. The overall deformation of the roadway surrounding rock is substantial, severely affecting roadway ventilation and personnel passage.

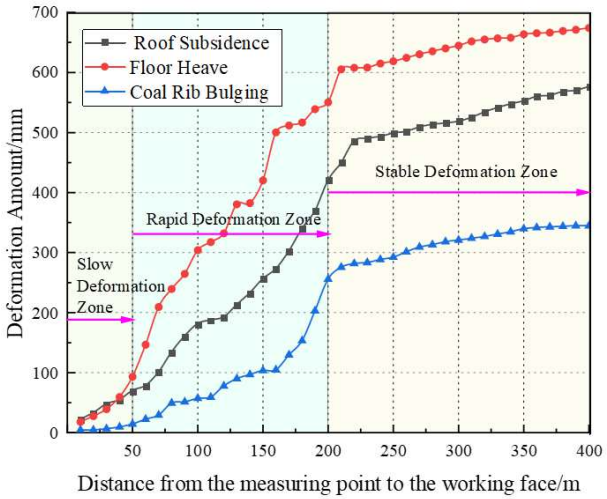


Figure 5. In-situ deformation curves of the roof and floor along the goaf-side roadway

2.3 Analysis of Gob-Side Roadway Instability and Its Control Methods

(1) High-stress instability: In gob-side entry retaining, the roof strata exhibit high strength and are difficult to fracture and collapse, resulting in a long-span cantilever roof in the gob area. This long-span cantilever bears a substantial portion of the overburden load, and as it rotates and subsides, it exerts severe compression on the retained entry. Consequently, the entry remains in a persistently high-stress environment, leading to large deformation and instability of the roof, floor, and sidewalls, as well as severe bending failure of the roof support beams.

(2) Compression-shear failure: In gob-side entry retaining within thick coal seams, the high stress induced by the rotation and subsidence of the hard roof, combined with the weak nature of the floor coal, results in uneven settlement of the coal floor beneath

the backfill body. This uneven settlement subjects the backfill body to horizontal shear forces. The larger the tilting deformation angle of the backfill body, the greater the shear force it experiences. Given that concrete backfill is “strong in compression but weak in shear”, shear action rapidly degrades its strength. Moreover, its early strength is insufficient, eventually leading to failure under compression-shear conditions and loss of load-bearing capacity, as shown in Figure 6.

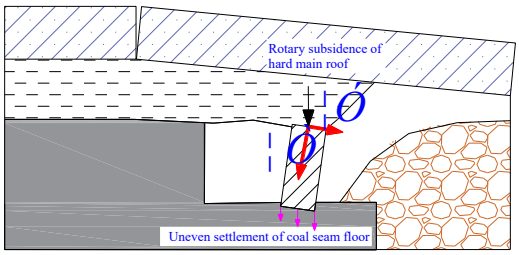


Figure 6. Schematic diagram of backfill body tilting in gob-side entry retaining

(3) Instability due to insufficient support strength: Substantial bulging and failure of roof bolts/cables occur on the roof adjacent to the backfill side. The bottom of the coal sidewall exhibits severe bulging, while the upper portion shows only minor deformation. The roof and sidewall exhibit asymmetric deformation, attributable to an uneven stress distribution within these strata. Stress concentration near the backfill area in both the roof and the bottom of the coal sidewall leads to insufficient support strength in this region, resulting in deformation and failure.

(4) Surrounding rock control method for gob-side entry retaining in thick coal seams with a hard roof: Based on the foregoing analysis of deformation and instability, and to address the issues of strong stress disturbance produced by an extended cantilever hard roof, insufficient compressive and shear strength of the backfill body, and localized inadequate support capacity, a collaborative control method of "pressure relief–support–backfilling" for gob-side entry retaining in thick coal seams with a hard roof is proposed. This method comprises three measures: roof cutting for pressure relief, deformation-coordinated support, and enhancement of the backfill body's compressive–shear resistance and rapid resistance increase. The core objective is to realize directional fracturing of the hard roof, as shown in Figure 7.

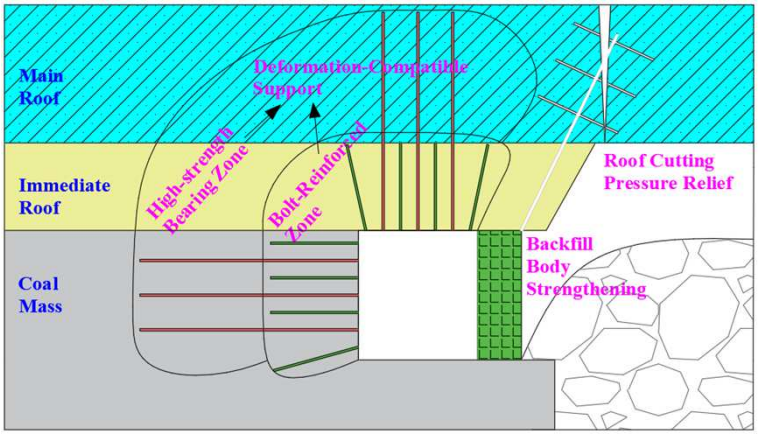
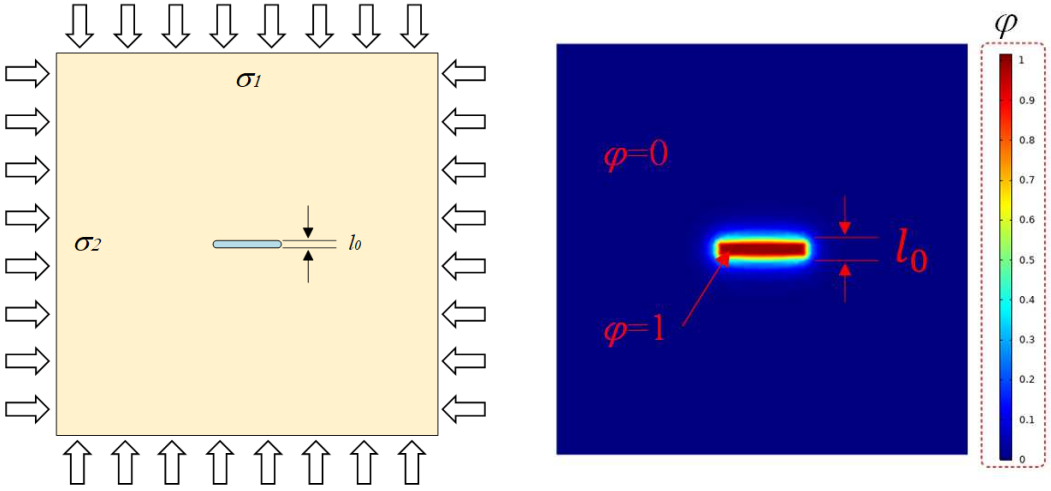


Figure 7. Schematic diagram of the "pressure relief–support–backfilling" collaborative control method for gob-side entry retaining in thick coal seams with a hard roof.

3 Numerical Simulation and Parametric Analysis of Hydraulic Fracture Propagation

3.1 Establishment of the numerical model and scheme

In this simulation, a phase-field model for hydraulic fracture propagation is established using COMSOL Multiphysics. Unlike the complex fracture propagation patterns in the fluid–solid coupling of PFC, the phase-field method introduces a phase-field function $\varphi(x,t)$ to confine fracture propagation within a certain region. The value of $\varphi(x,t)$ ranges from [0, 1], numerically representing the process from an unfractured state to a completely fractured state. The fracture width l_0 in the phase field actually corresponds to the portion of $\varphi(x,t)$ transitioning from 0 to 1, indicating the region undergoing fracturing, as shown in Figure 8.



(a) (b)

Figure 8. Schematic diagram of the fracture model

The model in this paper is established with reference to the phase-field fracture theory, governing equations, and other key parameters from [29], as well as Biot's theory of porous elastic media. The phase-field model is formulated by modifying the Helmholtz governing equation. To investigate the propagation of hydraulic fractures in rock strata and their propagation morphology when encountering natural fractures, initial conditions can be introduced to construct hydraulic fractures and natural fractures. The initial condition $H_0(x)$ is:

$$H_0(x)=\begin{cases}\dfrac{BG_c}{2l_0}\left[1-\dfrac{2d(x,l)}{l_0}\right], d(x,l)\le\dfrac{l_0}{2}\\ 0 \qquad\qquad\qquad\quad , d(x,l)>\dfrac{l_0}{2}\end{cases} \tag{1}$$

where B can take a value of 1×10^3, G_c is the critical fracture energy density, $d(x,l)$ is the distance from the point to the fracture, and l_0 is the fracture width.

At the two-dimensional and three-dimensional levels, the fracture density γ per unit volume can be expressed by the phase field and its gradient as follows:

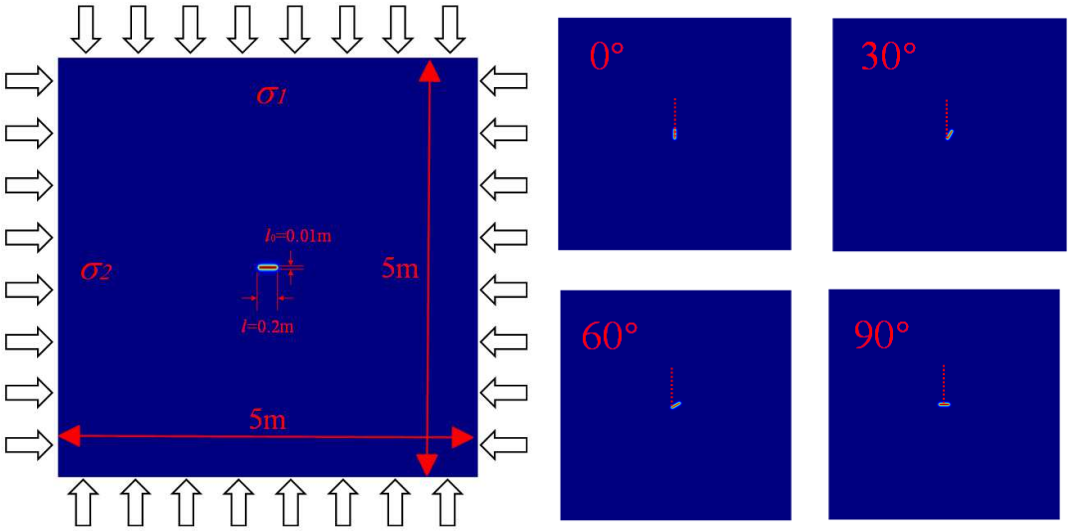
$$\gamma(\varphi,\nabla\varphi)=\frac{\varphi^2}{2l_0}+\frac{l_0}{2}\nabla\varphi\cdot\nabla\varphi \tag{2}$$

The in-situ stress environment is a key factor influencing hydraulic fracture propagation. To investigate the effects of different boundary stress ratios (σ_1/σ_2) and the angle between the in-situ stress and the notch direction on fracture propagation, the following numerical simulations were designed:

Simulation 1: σ_2 = 10MPa, σ_1/σ_2 ranging from 1.0 to 3.0 with a gradient of 0.2.

Simulation 2: σ_1 = 20MPa, σ_2 = 10MPa, a numerical simulation scheme with angles between the maximum principal stress and the fracture of 0°, 30°, 60°, and 90°.

The target rock stratum is sandstone. A 5 m × 5 m hydraulic fracture propagation model was established in COMSOL Multiphysics, as shown in Figure 9. The initial fracture length is 0.2 m, and the fracture width l_0 is 0.01 m. The simulated mass source is 100 kg/(m³·s), with boundary stresses σ_1 and σ_2 applied. The simulation parameters refer to the results of laboratory coal–rock mechanical tests, as listed in Table 1.



(a) Simulation 1 (b) Simulation 2

Figure 9. Model diagram of the hydraulic fracturing scheme

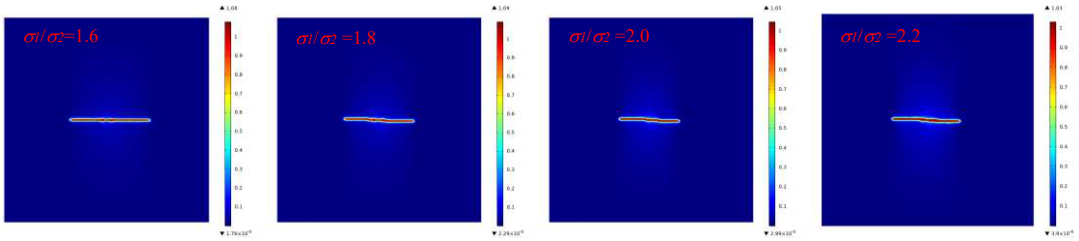
Table 1. Hydraulic fracturing simulation parameters

parameter	value	parameter	value
shear modulus μ	9.98GPa	model parameter $0< k \ll 1$	1e-9
elastic modulus λ	40.65GPa	Density ρ	2450kg/m^3
critical fracture energy density G_c	2700N/m	fracture aperture l_0	0.01m

3.2 Propagation laws of hydraulic fractures under different in-situ stresses

(1) Influence of boundary stress ratio on hydraulic fracture propagation.

The simulation results are presented in Figure 10. As the σ_1/σ_2 ratio increases, the hydraulic fracture remains undeflected for ratios below 2.2, whereas lateral extension becomes progressively evident. When the ratio reaches 2.4 or higher, the fracture deflects markedly toward the direction of the larger stress.



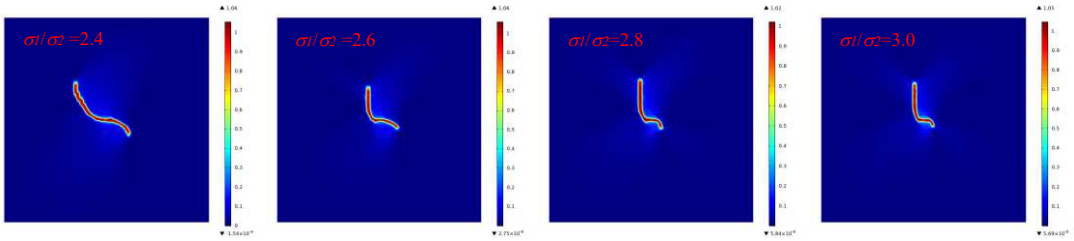


Figure 10. Fracture propagation diagrams under different boundary stress ratios

(2) Influence of the angle between the notch direction and the maximum principal stress on hydraulic fracture propagation

As shown in Figures 11 and 12, the final deflection trajectory of the fracture is directed toward the direction of the maximum principal stress. When the angle between the notch direction and the maximum principal stress increases from 0° to 90°, at 0° the fracture propagates directly along the notch direction; at 30° and 60°, deflection occurs; at 90°, deflection is not significant. As the angle increases, the peak water pressure and the peak location shift to the right, indicating greater difficulty in fracture propagation and deflection and requiring higher water pressure. Nevertheless, the fracture can still propagate effectively along the notch direction.

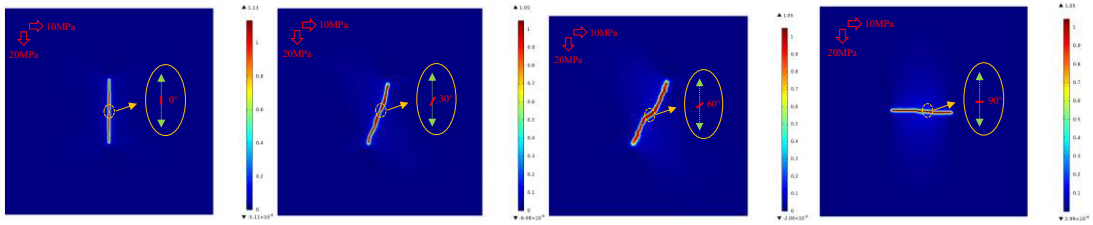


Figure 11. Propagation diagrams of fractures at different angles between the fracture and the maximum principal stress

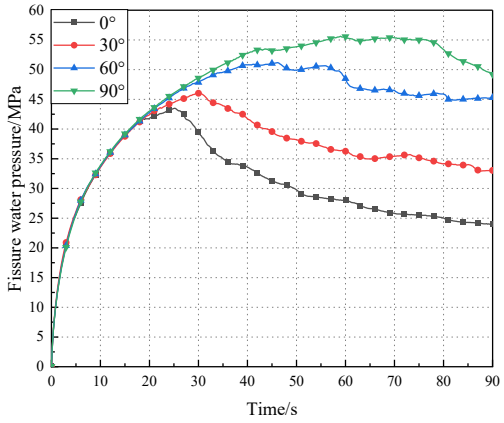


Figure 12. Water pressure diagrams of fractures at different angles

3.3 Propagation laws of hydraulic fractures encountering natural fractures

During the formation of rock strata, natural fractures are inevitable under the influence of multiple factors. In hydraulic fracturing, artificially induced fractures propagate under water-injection pressure and intersect natural fractures at varying orientations α, resulting in the co-propagation of fracture branches. As fluid infiltrates and pore pressure rises, two propagation modes are initially activated: propagation along the tips of natural fractures and penetration through natural fractures. These modes may subsequently re-emerge, ultimately forming a multi-fracture network, as illustrated in Figure 13.

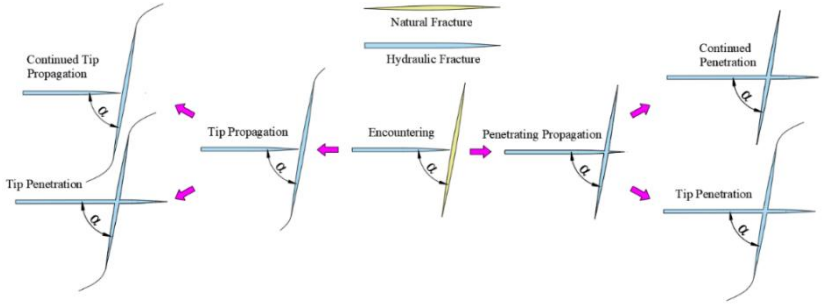


Figure 13. Schematic diagram of a hydraulic fracture encountering a natural fracture

To investigate the propagation behavior of hydraulic fractures when encountering natural fractures at different angles, a variable-angle hydraulic fracture–natural fracture interaction model was established in COMSOL Multiphysics (see Figure 14). The fracture length is 1 m, and the fracture width l_0 = 0.02 m. By adjusting the angle of the right fracture, the encountering angles between the hydraulic fracture and the natural fracture are set to 90°, 75°, 60°, 45°, 30°, 15°, and 0°, respectively. Horizontal and vertical stresses are applied at the boundaries, with σ_2 = 10 MPa and σ_1 = 24 MPa, to observe fracture propagation.

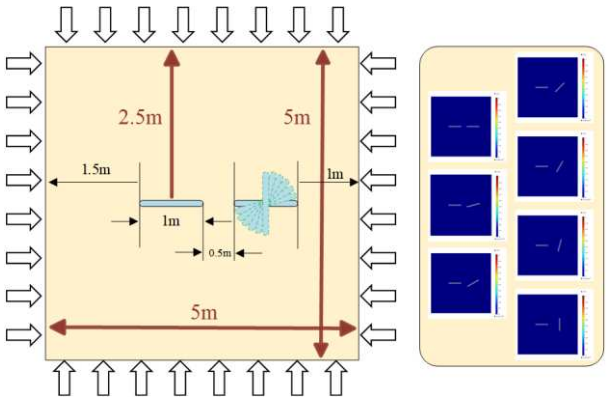
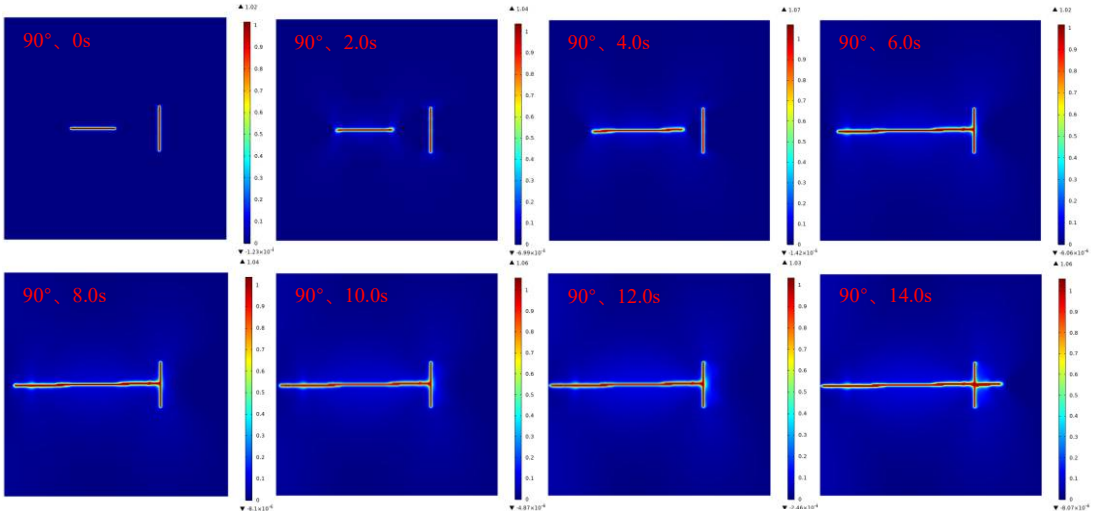


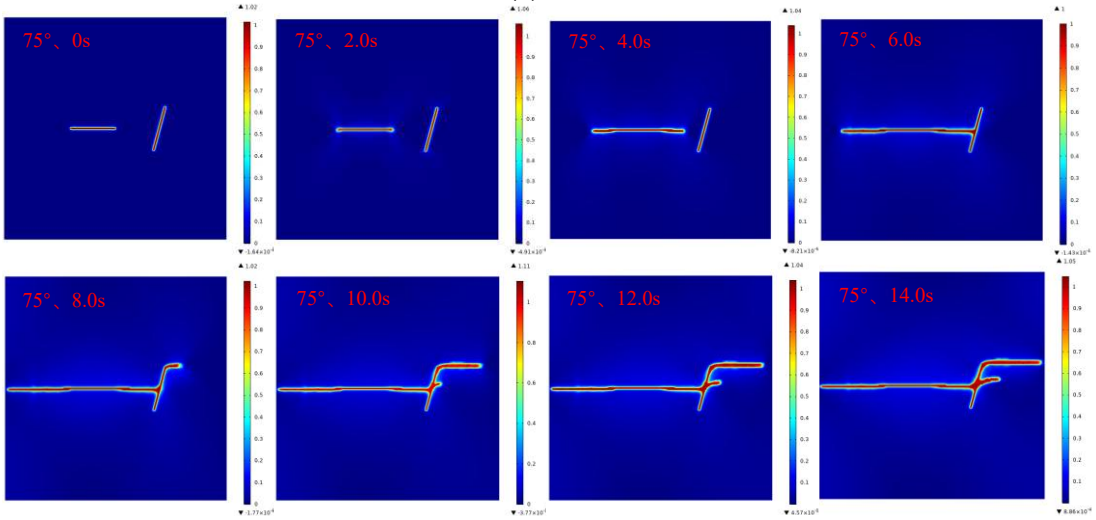
Figure 14. Numerical model diagram

The simulation timeline from 0 to 14 s is presented at 2 s intervals. Figure 15 shows that when the hydraulic fracture intersects a natural fracture at 90°, the injected fluid penetrates the natural fracture during propagation, forming a penetrating fracture. The penetrating fracture subsequently propagates without tip extension, indicating a relatively low energy requirement for penetration propagation in this configuration. At a 75° encounter, tip propagation occurs from 6 to 8 s, transitioning to penetration propagation from 8 to 10 s, and culminating in a combined tip+penetration propagation mode, implying an increasing energy demand for tip propagation over time. As tip propagation continues, once the energy threshold for penetration propagation is reached, both modes operate concurrently. For other encounter angles, only sustained tip propagation is observed without penetration, indicating that the energy for tip propagation remains consistently lower than that for penetration at small angles. Thus: (1) Penetration propagation is more favorable as the encounter angle approaches 90°, whereas tip propagation tends to dominate at smaller angles; (2) Fracture growth follows the path of least energy. Under certain stress states, near-perpendicular encounters require less energy for penetration propagation, whereas in most other cases, tip propagation requires less energy and dominates.

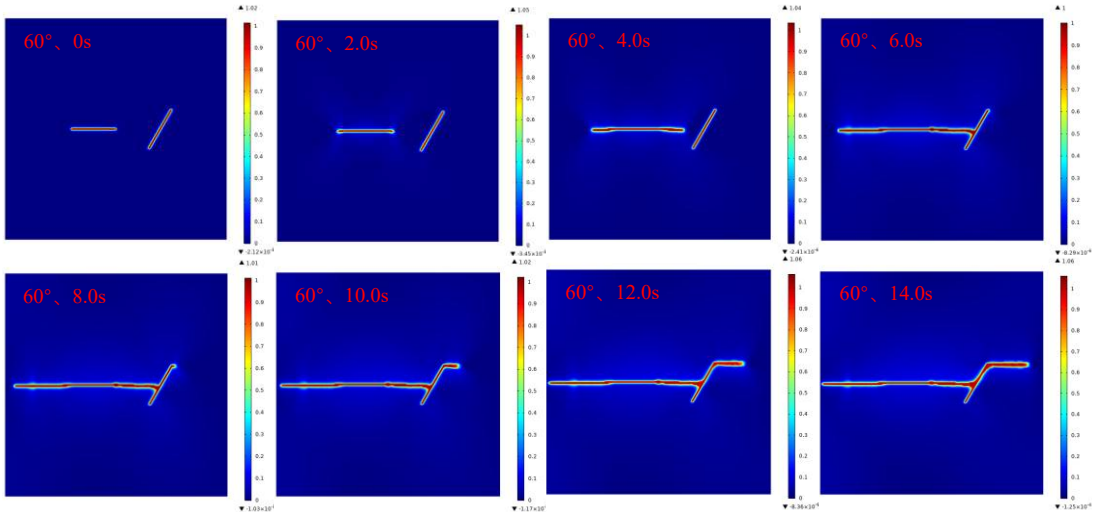
From the fracture water pressure shown in Figure 16, the pressure peaks near 2.5 s. However, Figure 15 indicates that the fracture has already propagated by t = 2 s, indicating that the initial rupture does not coincide with the peak pressure; hydraulic fracture initiation occurs during the rising-pressure phase, and the peak is reached only after the initial fracture has progressed. When the pressure falls sharply, it signals that the hydraulic fracture has begun to encounter the natural fracture, and the ingress of fluid into the natural-fracture cavity causes a sudden pressure drop. The timing of this drop varies with the encounter angle. In the simulation, rotating the natural fracture about its center causes an earlier encounter at smaller angles. After the pressure drop, the pressure gradually recovers, and the propagation enters a slow-growth and then stable stage. Notably, only at a 75° encounter does the subsequent water pressure exhibit a small reduction or stabilization, possibly because in the combined tip+penetration propagation regime, the energy is governed by the lesser of the two modes, so the overall energy demand no longer increases.



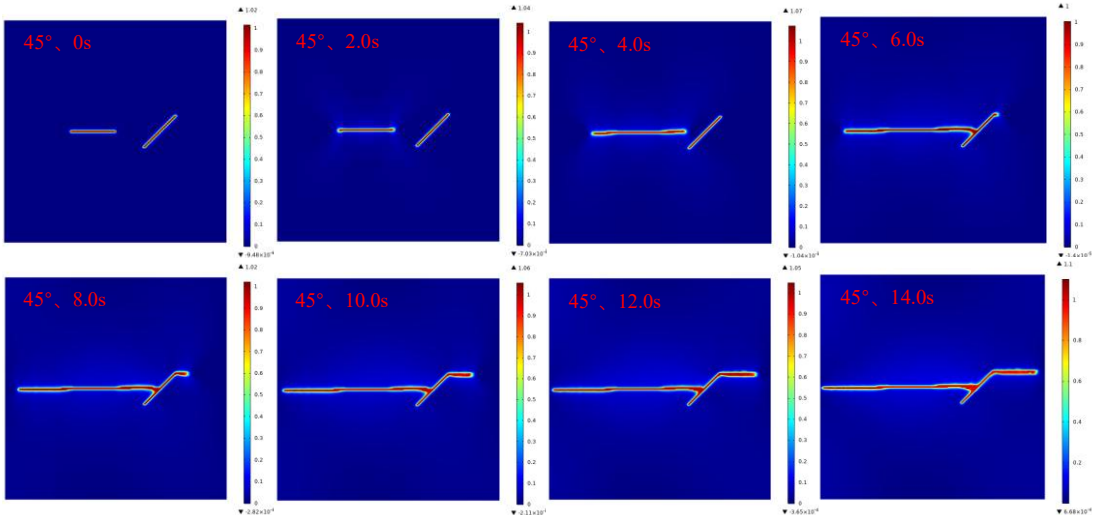
(a) 90°



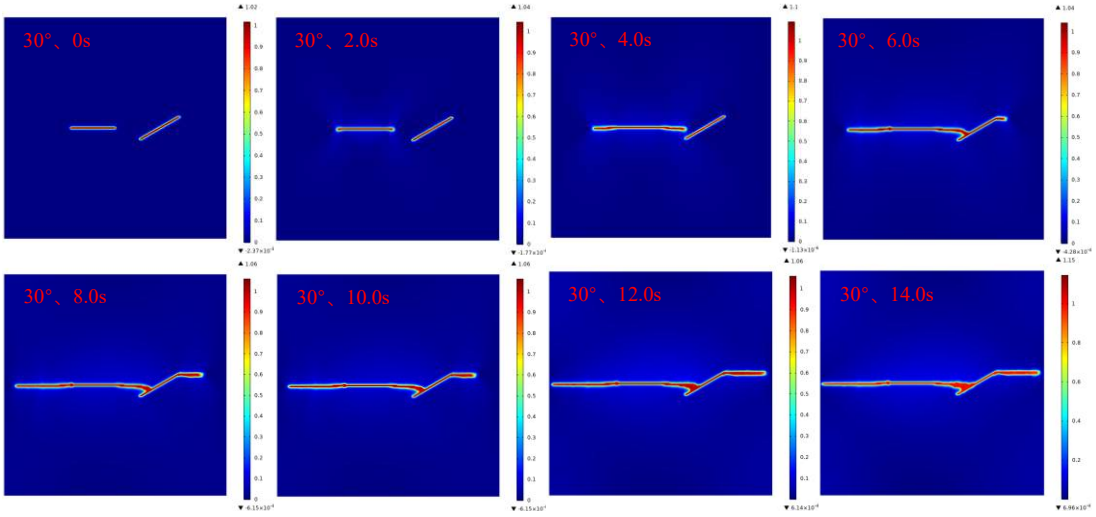
(b) 75°


60°、0s
60°、2.0s
60°、4.0s
60°、6.0s
60°、8.0s
60°、10.0s
60°、12.0s
60°、14.0s

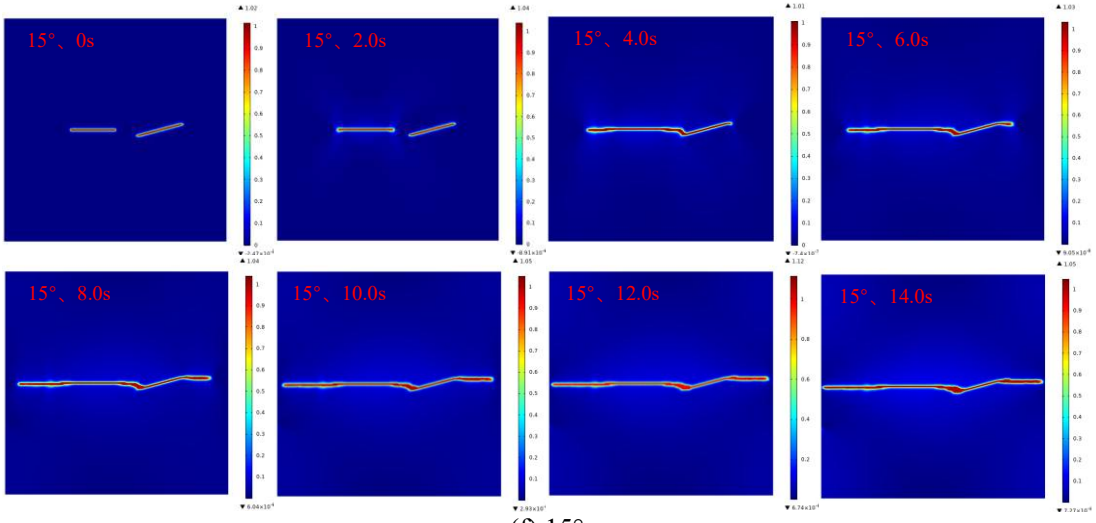
(c) 60°


45°、0s
45°、2.0s
45°、4.0s
45°、6.0s
45°、8.0s
45°、10.0s
45°、12.0s
45°、14.0s

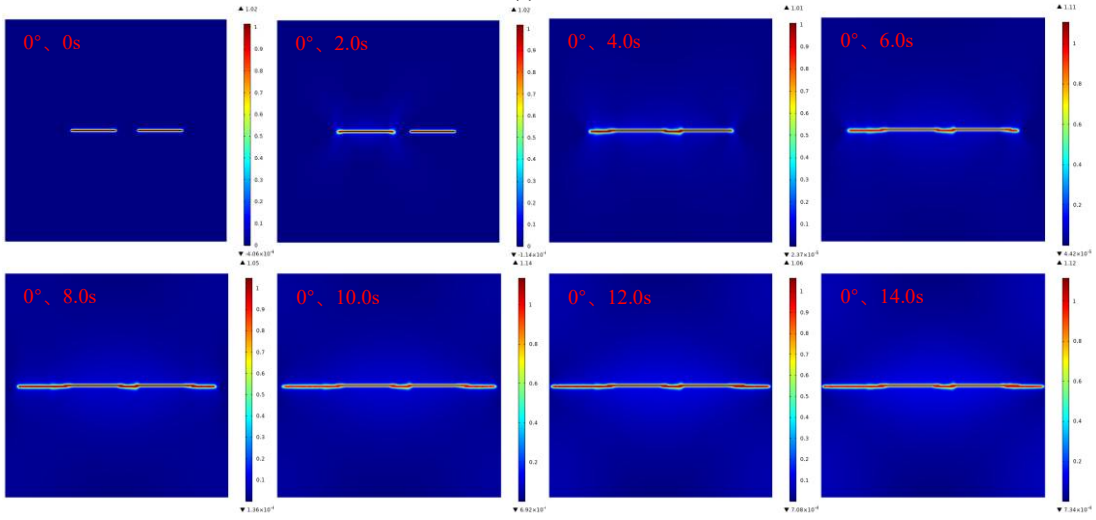
(d) 45°


30°、0s
30°、2.0s
30°、4.0s
30°、6.0s
30°、8.0s
30°、10.0s
30°、12.0s
30°、14.0s

(e) 30°



(f) 15°



(g) 0°

Figure 15. Propagation diagrams of a hydraulic fracture encountering a natural fracture

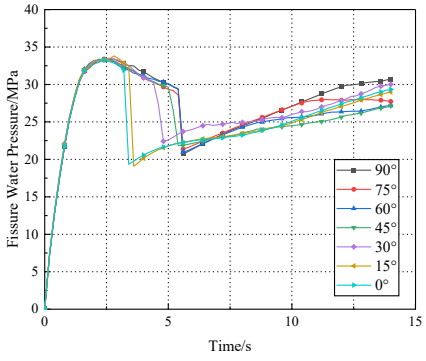


Figure 16. Water pressure diagrams of fractures at different encounter angles

3.4 Determination of Roof Cutting Pressure Relief Parameters

In hydraulic fracturing operations, the roof-cutting angle α should be neither excessively large nor small, and is typically taken in the range of 10°–20°. The length of the injection steel pipe during roof cutting is 1.5 m, and the cutting height h is selected in increments of 1.5 m. To examine the influence of different roof-cutting angles and cutting spacings on fracture propagation, nine parameter sets were considered: α = 10°, 15°, 20°; h = 1.5 m, 3.0 m, 4.5 m, where H denotes the roof-cutting height. To determine the optimal parameter combination, numerical simulations were

established as shown in Figure 17. All nine configurations were simulated within a model domain of 20 m × 20 m and a roadway cross-section of 6 m × 3.8 m. Based on in situ stress measurements from the Gucheng Coal Mine, the boundary stresses were prescribed as σ_2 = 14 MPa and σ_1 = 19 MPa, and the results after 30 s of simulation were used as the benchmark. By examining the fracture propagation for each configuration, the set exhibiting the most favorable propagation was identified as the optimal parameter combination.

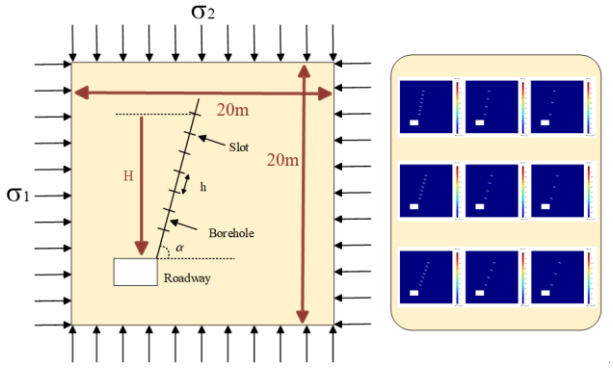
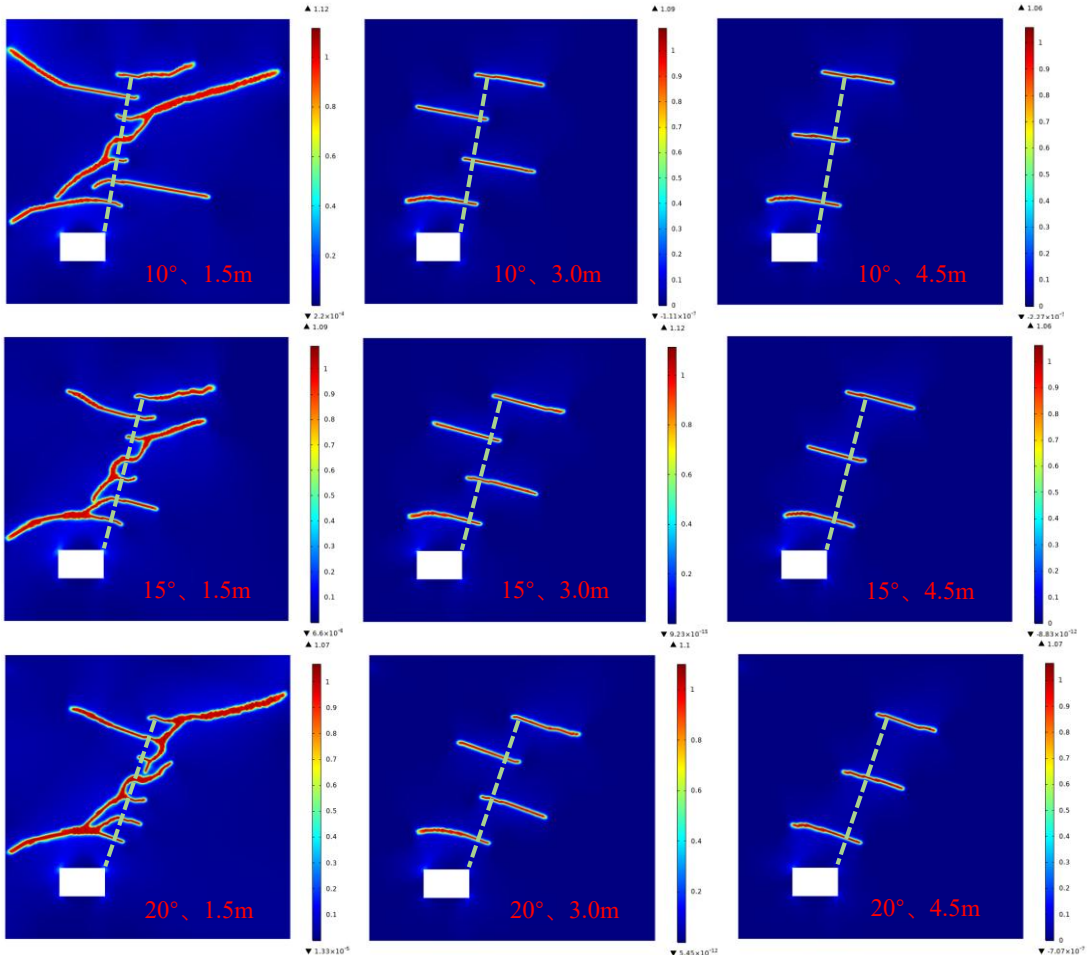


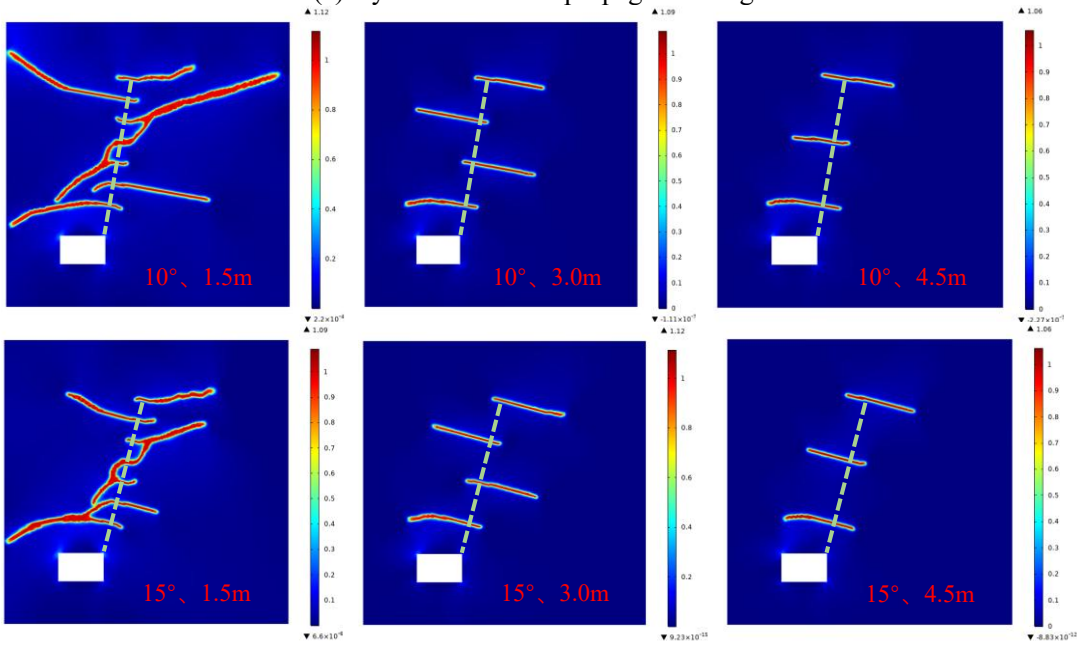
Figure 17. Model diagram of roof cutting

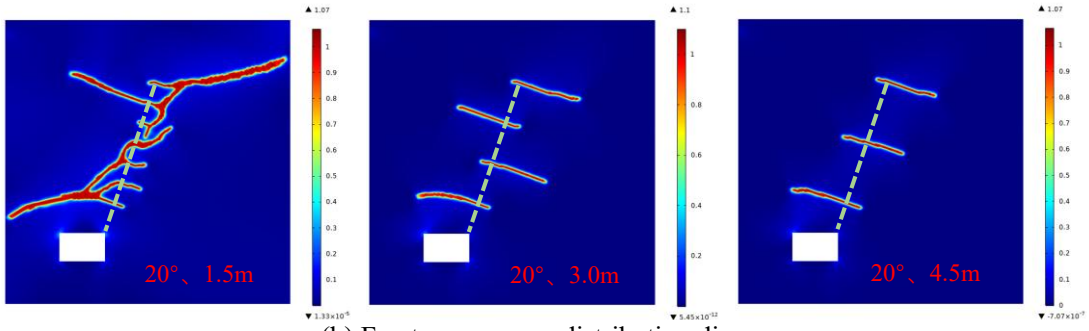
Simulation results presented in Figures 18(a) and 18(b) indicate that when the spacing between fracturing points is 1.5 m, fracture pressures corresponding to different roof-cutting angles interfere and overlap, causing fractures to deviate from the intended directions and, in some cases, propagation paths to intersect. This markedly reduces the utilization efficiency of the fracturing notches and increases nonproductive work. At a spacing of 3.0 m, fracture-pressure distributions begin to delineate themselves, with relatively small local mutual influences. The propagation paths align well with the intended directions, but the fractures exhibit pronounced staggered propagation, which weakens the thinning effect on a single flank of the rock layer. When the spacing is 4.5 m, the fracture pressures become independent, and the propagation paths and arrangements conform to the design; therefore, spacings ≥4.5 m yield the best fracturing effect.

Regarding the roof-cutting angle, variation in the angle is small, and fracture propagation remains comparatively uniform. At a 20° angle, propagation and arrangement show strong consistency, with effective roof-cutting effects on both sides. Moreover, for all tested roof-cutting angles, the fractures initially propagate a finite length along the notch direction and then deflect toward the direction of the horizontal maximum principal stress, thereby achieving directional hydraulic fracturing of the roof. Compared with hydraulic fracturing without a notch, notched hydraulic fracturing affords better control of the crack initiation direction and subsequent propagation, and requires a lower initiation water pressure, making it more favorable for implementing roof-cutting operations.



(a) Hydraulic fracture propagation diagram





(b) Fracture pressure distribution diagram

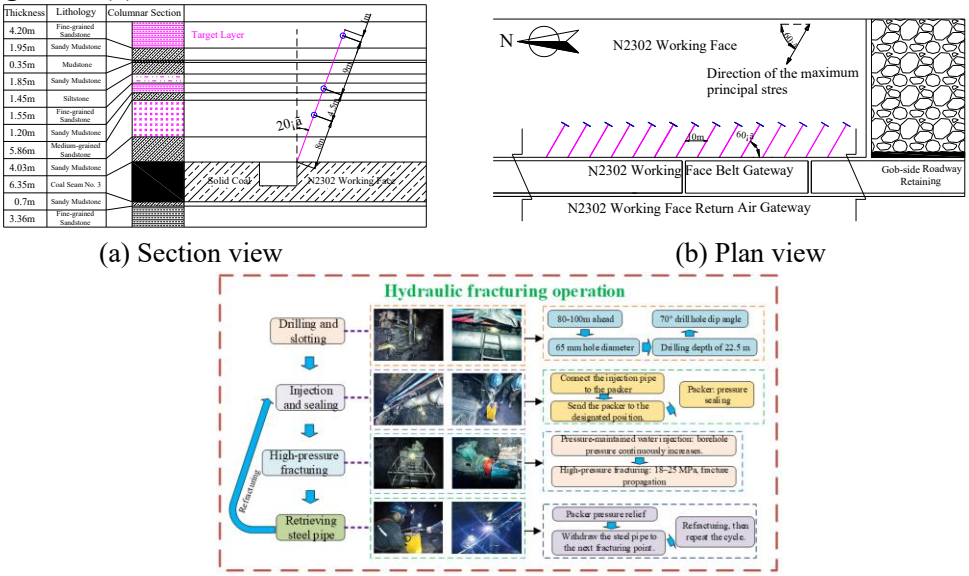
Figure 18. Hydraulic fracture propagation and pressure distribution diagrams under different roof cutting angles and spacings

4 On-site engineering application

4.1 Surrounding rock control scheme for gob-side entry retaining

(1) Roof cutting pressure relief scheme

Based on in-situ stress test results and the borehole columnar section of the Gucheng Coal Mine, the mining height of the N2302 working face is 6.35 m. A bulking coefficient of 1.3 is adopted, yielding a caving height required to fill the gob of 21.2 m. Under the specified surrounding rock conditions, the roof-cutting height H is taken as 22 m. The working face is controlled by a strike-slip fault stress field characterized by $\sigma_H > \sigma_v > \sigma_h$, with the maximum principal stress approximately 19 MPa oriented about 60° north of west. In-situ stress markedly influences the deflection of hydraulic fractures during roof cutting. When the notch direction is perpendicular to the direction of the in-situ stress, fracture deflection is more difficult, which is favorable for directional propagation. To reduce the integrity of the rock stratum, the boreholes in this test were arranged at an elevation angle of 70° and an angle of 60° with respect to the working face. The borehole diameter is 65 mm, and the borehole depth is 22.5 m. Hydraulic fracturing was performed three times, with fracturing points located at distances of 8 m, 12.5 m, 18.5 m, and 21.5 m from the borehole orifice. The borehole layout is shown in Figures 19(a) and 19(b), and the implementation process is shown in Figure 19(c).



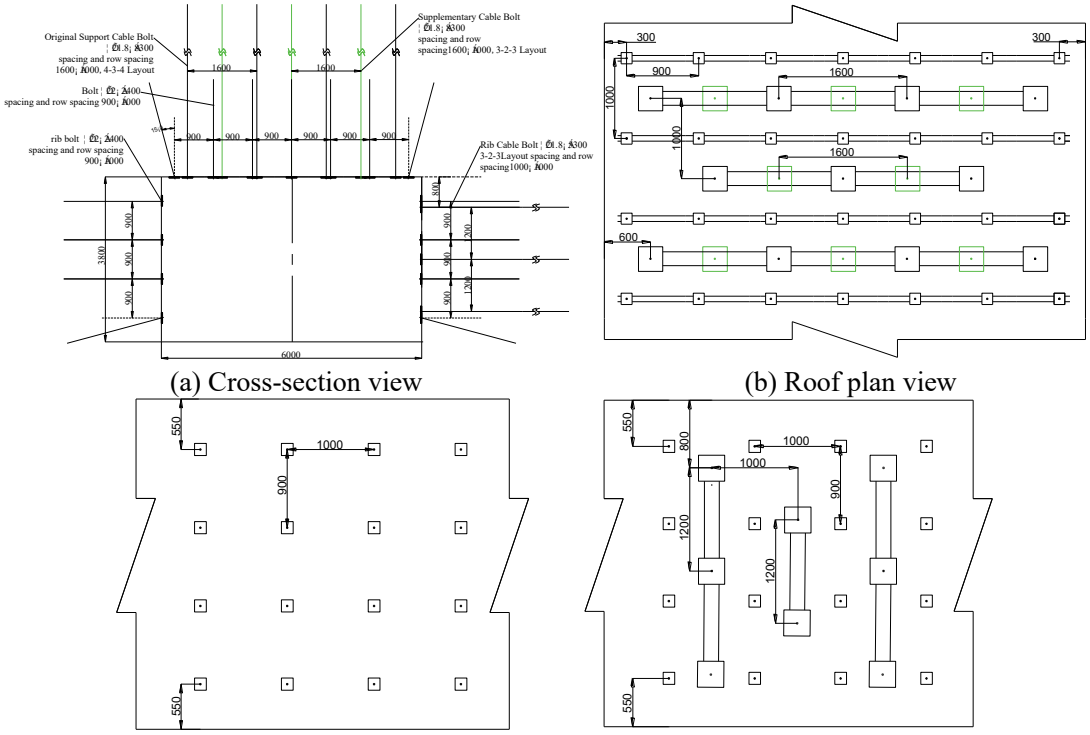
(a) Section view (b) Plan view

(c) Field implementation

Figure 19. Hydraulic fracturing scheme and field construction diagram

(2) Optimisation of in-roadway support scheme

The optimised support scheme is presented in Figure 20. Rock bolts: Φ22 × 2400 mm (diameter × length). Roof bolts are arranged with a spacing of 900 × 1000 mm, with seven bolts per row; sidewall bolts are arranged with a spacing of 900 × 1000 mm, with four bolts per row. The pre-tension force of each bolt is 70 kN. Roof cables: Φ21.8 × 8300 mm (diameter × length), spacing 1600 × 1000 mm, arranged in a 4-3-4 pattern. Additional reinforcement cables are arranged with a spacing of 1600 × 1000 mm in a 3-2-3 pattern. The pre-tension force of each cable is 300 kN. Coal sidewall: Sidewall cables of Φ21.8 × 5300 mm (diameter × length), spacing 1200 × 1000 mm, arranged in a 3-2-3 pattern.



(a) Cross-section view (b) Roof plan view

(c) Gob side (d) Solid coal side

Figure 20. Support diagram of the optimised belt roadway

(3) Performance enhancement and anti-tilt design of the backfill body

The roadside backfill body was prepared with a water-cement ratio of 0.5, an early strength agent content of 0.6%, and a fibre content of 0.3%. This formulation significantly improves the early strength, while the fibres enhance the crack resistance and the compressive-shear capacity of the backfill, thereby increasing its strength and stability. The mechanical model indicates that after roof cutting for pressure relief, the width of the backfill wall can be optimised from 1.5 m to 1.2 m. Owing to the soft floor coal, which has low bearing capacity and is prone to deformation, the backfill body tends to tilt. To improve the anti-tilt and compressive-shear capability, foundation reinforcement was implemented at the bottom: a concrete foundation was cast by pre-trenching, with dimensions of 1.0 m × 2.0 m (see Figure 21(a)). This increases the contact area with the floor coal, reduces the bearing pressure at the bottom, and mitigates tilting. In combination with temporary support consisting of a one-beam-three-prop large plank shed, tie bolts were installed on the flexible formwork. Steel strips, pallets, and bolts were placed at both ends of the tie bolts, with a bolt

spacing of 800 mm × 900 mm (as shown in Figure 21(b)), to enhance the supporting resistance of the backfill body. Based on the results of backfill material tests, field backfilling tests were conducted. The construction process and field implementation of the flexible-formwork concrete for the N2302 transport cross-heading are shown in Figure 21(c).

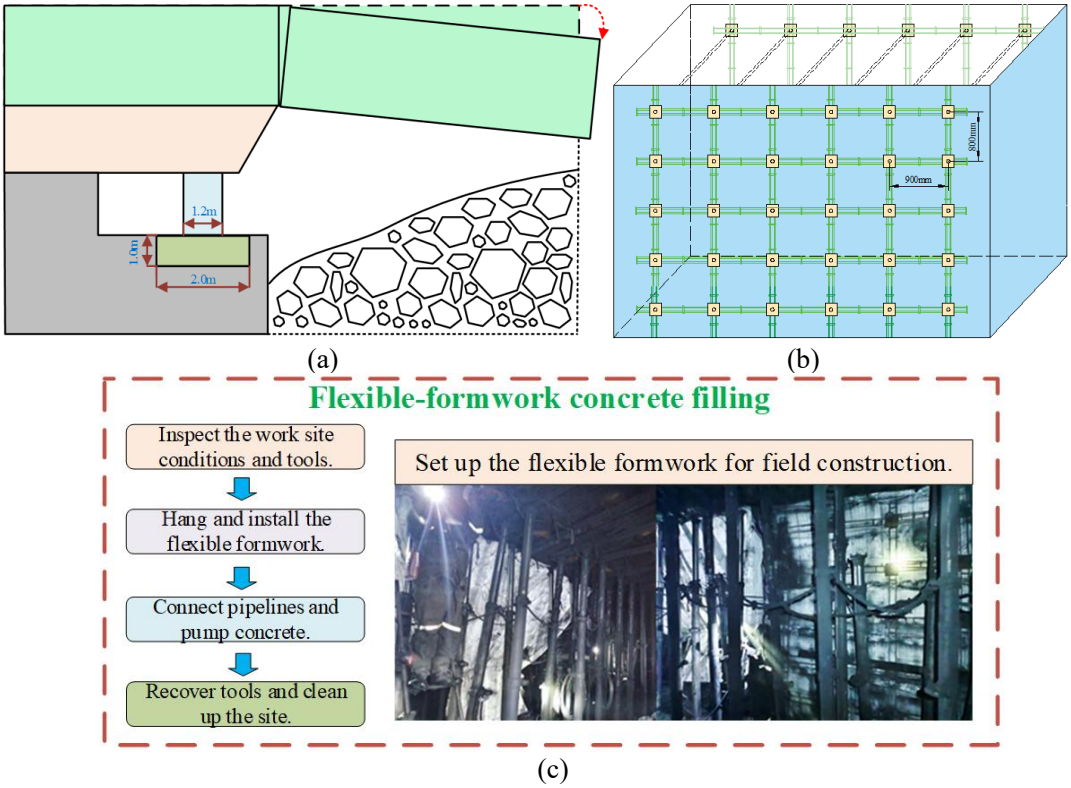


Figure 21. Performance optimisation and anti-tilt scheme of the backfill body

4.2 Monitoring and Analysis of Surrounding Rock Control Effect in the Roadway

Site observations of surrounding rock displacement and the effectiveness of control in the roadway construction section are presented in Figures 22 and 23. Compared with the scheme without the 'pressure relief–support–backfilling' collaborative control, the results show reductions in roadway surrounding rock displacements across all three stages, albeit to varying degrees. Notably, floor heave remains the largest deformation relative to roof subsidence and coal sidewall bulging, but it decreases from 670 mm to approximately 290 mm, a substantial reduction. Roof subsidence and coal sidewall bulging are also reduced from 580 mm and 340 mm to about 230 mm and 180 mm, respectively. The overall deformation control of the roadway is satisfactory. Field photographs corroborate that the backfill body maintains a robust supporting geometry without signs of bulging failure; the coal sidewall exhibits no obvious bulging; the roadway profile remains well-preserved, and the support components operate normally without evident signs of failure or damage. These observations meet the requirements for normal mining operations. The collaborative 'pressure relief–support–backfilling' control of the roadway achieves favorable overall results, with a pronounced effect on surrounding rock control.

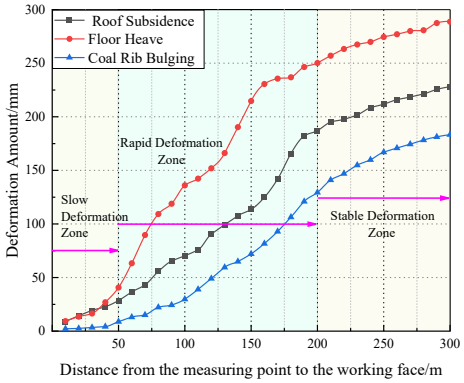


Figure 22. Displacement variation diagram of the surrounding rock in the gob-side entry retaining



(a) Backfill side (b) Overall effect

Figure 23. Surrounding rock control effect diagram of gob-side entry retaining

5 Conclusion

This study addresses the challenges associated with gob-side entry retaining in thick coal seams with a hard roof, including difficult support, elevated surrounding rock stress concentrations, and inadequate stability of the roadside backfill body. A collaborative control strategy for gob-side entry retaining in thick coal seams with a hard roof—"pressure relief–support–backfilling"—with directional hydraulic fracturing as the core technique is proposed. The advantage of this method lies in its multi-faceted, collaborative stabilization of gob-side entry retaining. The main conclusions distinguishing this work from prior studies are as follows:

(1) The deformation and failure characteristics of GER in thick coal seams with a hard roof were revealed, including long cantilever hanging, compression–shear failure of the backfill, and localized insufficient support. A collaborative "pressure relief–support–backfilling" method was proposed.

(2) COMSOL phase-field simulations clarified hydraulic fracture propagation under in-situ stress ratios, natural-fracture intersection angles, and cutting parameters. The optimal parameters are fracture spacing ≥4.5 m, cutting angle 20°, and boreholes aligned with the maximum horizontal principal stress.

(3) The N2302 field trial showed that floor heave, roof subsidence, and rib convergence decreased from 670/580/340 mm to 290/230/180 mm, respectively, confirming the effectiveness of the proposed method.

Author contribution.

Zhijun Xu: Writing—original draft; Chong Li: Funding acquisition, Writing—review and editing; Shuaishuai Jiang: Data curation; Xinlong Ma: Visualization; Yadong Zheng: Supervision; Yue Cao:

Funding acquisition, Investigation.

Funding: This work was supported by the National Natural Science Foundation of China(No.52374140), (No.52404147).

Institutional Review Board Statement: Not Applicable.

Informed Consent Statement: Not Applicable.

Data Availability Statement: The datasets used and/or analysed during the current study are available from the corresponding author on reasonable request.

Conflicts of Interest: The authors declare no conflict of interest.

References

[1] Kang H, Jiang P, Wu Y, et al. A combined “ground support-rock modification-destressing” strategy for 1000-m deep roadways in extreme squeezing ground condition[J]. International Journal of Rock Mechanics and Mining Sciences, 2021, 142: 104746.

[2] He M, Wang Q, Wu Q. Innovation and future of mining rock mechanics[J]. Journal of Rock Mechanics and Geotechnical Engineering, 2021, 13(1): 1-21.

[3] Shen F , Song Y , Zhao W ,et al.Research on Novel Method of Gob-Side Entry Retaining Under the Synergistic Effect of Roof Cutting and Roadside Filling in Thick Coal Seams[J].Rock Mechanics & Rock Engineering, 2023, 56(10): 7217-7236.

[4] Zhuang J, Mu Z, Cai, WuHe, et al. Hydraulic fracturing of a horizontal well for hard roof-related coal burst control: Insights from numerical modelling to field application[J]. international journal of mining science and technology, 2024, 34(8):1095-1114.

[5] Geng D , Fan L , Du Y ,et al.Research on the mechanism and control of roof deformation in gob-side entry retaining of close-distance coal seams[J].Engineering Failure Analysis, 2024, 164(000):20.

[6] Yang J, Liu B, Wang YJ, et al.Roof control mechanism and partition compensation support technology of gob-side entry formed by N00 mining method in thin coal seam[J].Journal of Central South University, 2024, 31(2):602-620.

[7] Dong Z, Qian Z, Jian B, et al.Theory and simulation investigations on stability control of gob-side entry retaining with coal pillar-backfill body system[J]. International Journal of Mining Science and Technology, 2025, 35(8): 1399-1417.

[8] Zhang Z, Deng M, Bai J, et al.Stability control of gob-side entry retained under the gob with close distance coal seams[J].International Journal of Mining Science and Technology, 2021, 31(2):321-332.

[9] Guo J S, Ma L Q, Ngo I Mechanism and control of deformation in gob-side entry with thick and hard roof strata[J].The Journal of The Southern African Institute of Mining and Metallurgy, 2023, 123(8):423-434.

[10] Kang H, Jiang P, Feng Y, et al.Application of Large-Scale Hydraulic Fracturing for Reducing Mining-Induced Stress and Microseismic Events: A Comprehensive Case Study[J].Rock Mechanics and Rock Engineering, 2022, 56(2):1399-1413.

[11] Wang B, Zhou D, Zhang J.Research on deformation characteristics and control technology of surrounding rock for gob-side entry with small coal pillar in gently inclined coal seam[J].Energy Science & Engineering, 2024, 12(4):1759-1774.

[12] He W R, Zhai W L, He F L Mechanism and scientific parameters of pressure relief by cutting key blocks above gob-side entry in extra-thick coal seam: A case study[J].Journal of Central South University, 2026, 33(2):703-724.
[13] Zhao H, Zhang B, Gao L, et al.Static Blasting Roof Cutting Surrounding Rock Control Technology for Narrow Coal Pillar Gob-Side Entry Driving in Thick Coal Seams[J].International Journal of Geomechanics, 2025, 25(6).
[14] Zou J , Zhang Q , Jiang Y ,et al.Mechanism of hydraulic fracturing for controlling strong mining-induced earthquakes induced by coal mining[J].International Journal of Rock Mechanics and Mining Sciences, 2024:181.
[15] Xia B , Ma Z , Zhou L ,et al.Decoding the Hard Roof Control Mechanism of Ground Fracturing Based on the Material Point Method[J].Rock Mechanics and Rock Engineering, 2025, 58(8):8721-8736.
[16] Gao R , Bai D , Yu B ,et al.Ground fracturing of multi-strata for strong ground pressure control in extra-thick coal seams with hard roofs: Numerical simulation and case study[J].Engineering Fracture Mechanics, 2024:303.
[17] Tian H , Jiang Z , Ma Z ,et al.Microseismic identification and effectiveness assessment of hydraulic-fracturing–induced roof cutting using an STFT–CNN framework[J].Journal of Applied Geophysics, 2026, 246(c):106078.
[18] Lyu S , Wang S , Li J ,et al.Massive Hydraulic Fracturing to Control Gas Outbursts in Soft Coal Seams[J].Rock Mechanics and Rock Engineering, 2022, 55(3):1759-1776.
[19] Wang M Z, Zheng H H, Ma Z Q, et al. Control Technology of Roof-Cutting and Pressure Relief for Roadway Excavation with Strong Mining Small Coal Pillar[J]. Sustainability, 2023, 15(3): 2046-2046.
[20] Huang X H, Zhang C, Ren Z P. Parameter determination and effect evaluation of gob-side entry retaining by directional roof cutting and pressure releasing[J]. Engineering Failure Analysis, 2024, 156, 107847-107863.
[21] Xu X D, Zhou Y J, Yang J, et al. An Innovative Mechanism of Directional Rock Cracking Mechanics and Mine Pressure Control Method for Energy-Gathering Blasting[J]. Rock Mechanics and Rock Engineering, 2024, 57(10): 8657-8677.
[22] Qin J L, Zhu P. Research on Roof Cutting and Pressure Relief Technology of Deep Hole Pre-cracking Blasting[J]. International Journal of Energy, 2024, 4(3): 6-10.
[23] Zhang X, Kang H P. Pressure Relief Mechanism of Directional Hydraulic Fracturing for Gob-Side Entry Retaining and Its Application[J]. Shock and Vibration, 2021(1): 6690654.
[24] Wang T, Xu G Y, Liu L Y, et al. Principle and practice of hydraulic softening, top-cutting and pressure relief technology in weakly cemented strata[J]. Frontiers in Earth Science, 2024, 12, 1367933.
[23] Cheng S , Wu B , Zhang X ,et al.How Energy Dissipation Mode Controls the Evolution of Multiple Plane-Strain Hydraulic Fractures Under Isotropic Stresses[J].Journal of Geophysical Research: Solid Earth, 2024, 129(8).
[24] Papachristos E , Scholtès , L , Donzé , F.V , et al.Intensity and volumetric characterizations of hydraulically driven fractures by hydro-mechanical simulations[J].International Journal of Rock Mechanics and Mining Sciences, 2017, 93:163-178.
[25] Zhang F , Wang X , Bai J ,et al.Fixed-length roof cutting with vertical hydraulic fracture based on the stress shadow effect: A case study[J].International Journal of Mining Science and

589 Technology, 2022, 32(2):295-308.
590 [26] He W R, Zhai W L, He F L Mechanism and scientific parameters of pressure relief by cutting
591 key blocks above gob-side entry in extra-thick coal seam: A case study[J].Journal of Central
592 South University, 2026, 33(2):703-724.
593 [27] Hou C， Ma N. Investigation of the stresses in the coal masses on both sides of a coal-seam
594 roadway and the limit-equilibrium zone. Journal of China Coal Society, 1989, (04): 21-29.
595 [28] Shen F. Research on Mechanism and Stability Control of Gob-side Entry Retaining Under the
596 Synergistic Effect of Roof Cutting and Roadside Filling in Thick Coal Seams[D]. China
597 University of Mining and Technology (Beijing), 2024.
598 [29] Zhou S, Zhuang X, Timon Rabczuk. A phase-field modeling approach of fracture propagation
599 in poroelastic media[J]. Engineering Geology, 2018, 240: 189-203.